Breathing mode dynamics of coupled three-dimensional chiral bobbers

P. Bassirian, [ID] T. Hesjedal, [ID] S. S. P. Parkin, et al.

COLLECTIONS

Paper published as part of the special topic on Science and Technology of 3D Magnetic Nanostructures

View Online   Export Citation   CrossMark

**ARTICLES YOU MAY BE INTERESTED IN**

The design and verification of MuMax3
AIP Advances **4**, 107133 (2014); https://doi.org/10.1063/1.4899186

Self-filtering narrowband perovskite photodetector with ultra-narrowband and high spectral rejection ratio
APL Materials **10**, 101109 (2022); https://doi.org/10.1063/5.0120959

Role of Al additions in secondary phase formation in CoCrFeNi high entropy alloys
APL Materials **10**, 101108 (2022); https://doi.org/10.1063/5.0117280
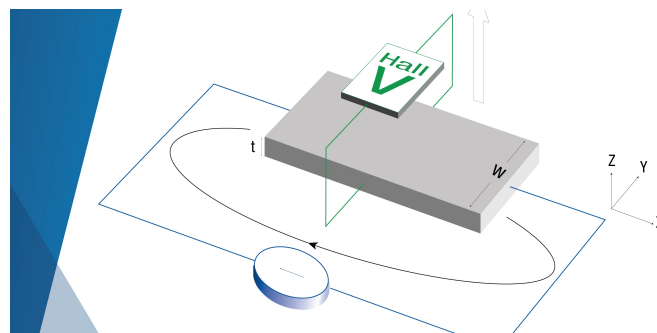
AIP Publishing

Breathing mode dynamics of coupled three-dimensional chiral bobbers

View Online   Export Citation   CrossMark

P. Bassirian,[1,2] T. Hesjedal,[1] (iD) S. S. P. Parkin,[2] (iD) and K. Litzius[3,a)] (iD)

AFFILIATIONS

[1] Department of Physics, Clarendon Laboratory, University of Oxford, Oxford OX1 3PU, United Kingdom
[2] Max Planck Institute of Microstructure Physics, Weinberg 2, 06120 Halle, Germany
[3] Max Planck Institute for Intelligent Systems, Heisenbergstrasse 3, 70569 Stuttgart, Germany

Note: This paper is part of the Special Topic on Science and Technology of 3D Magnetic Nanostructures.
[a)]Author to whom correspondence should be addressed: litzius@is.mpg.de

ABSTRACT

Recently, three-dimensional (3D) magnetic textures have moved into the focus of spintronics as both technologically relevant and physically intriguing on a fundamental level. A rich variety of 3D textures is currently being investigated; however, their unambiguous experimental detection and detailed study remains challenging. In this work, a new type of chiral 3D spin-texture, consisting of two antiferromagnetically coupled Néel bobbers, is explored. The static properties of this structure depend on the chirality of the individual bobbers. Different chirality combinations are studied with regard to their phase stability regions by micromagnetic simulations and compared to antiferromagnetically coupled skyrmion tubes. Furthermore, the coupled internal breathing modes are investigated by application of a periodically alternating external magnetic field. The breathing modes of each studied system possess a unique fingerprint, which might allow for the identification of the resonating spin textures via their dispersion curves.

I. INTRODUCTION

Magnetic skyrmions are topological, nanoscale spin structures, which are embedded in a ferromagnetic background, with their cores being polarized oppositely to the background. In general, they can be categorized by the symmetry of their domain walls into Néel- or Bloch-type skyrmions. Their chirality is determined by the Dzyaloshinskii–Moriya interaction (DMI), which can be present in non-centrosymmetric systems and which will result in left- or right-handed skyrmions. The specific symmetry of the DMI is related to its origin via the type of symmetry breaking within the system. Owing to their topological nature, skyrmions are particularly stable. Ever since skyrmions have been brought into focus as spintronic information carriers, a plethora of scientific activities have shed light on their static and dynamic behaviors.[1–4] Experimentally, Bloch skyrmions have been observed in a wide range of B20 materials,[5–7] while Néel skyrmions were predominantly observed and studied in ultrathin multilayers with broken inversion symmetry at the interfaces.[8–13] Note that Néel skyrmions were also reported in bulk systems with specific crystal symmetries[14,15] and as surface states of B20 crystals.[16]

Parallel to experimental research, a zoo of topological objects have been theoretically predicted, some of which emerge when extending the planar description of a skyrmionic excitation to the third dimension.[17] The simple stacking of skyrmions of the same size and chirality will, e.g., generate a skyrmion tube (also called a string).[18–21] More complex structures can be produced by twisting the string-like skyrmion or by connecting the ends to form a closed loop, which are often referred to as hopfions.[22–26] Such knotted magnetic structures can also be formed in systems with higher order magnetic interactions,[27] as well as in models of frustrated magnets, where they have been first predicted.[28]

Another three-dimensional topological soliton is the chiral bobber.[28–32] It can be imagined as a stack of skyrmions that continuously decrease in size, eventually terminating in a Bloch Point (BP)—a magnetic point singularity that can also, intriguingly, be described as a point-like quasi-monopole. In theory, bobbers can be readily generated by interfacing skyrmion-hosting materials with

a thin magnetic layer with high perpendicular magnetic anisotropy and high exchange stiffness. The interaction of this layer with the skyrmion hosting material causes a pinching off of the skyrmion tube. Most commonly, the additional layer is simply treated as a pinned layer with fixed uniform magnetization.[22,24] When a homogeneous skyrmion string is pinched off at both ends, two terminating BPs can be generated. These structures are referred to as torons,[24,33] monopole strings,[22] or dipole strings.[34,35] Note that the term dipole string is only used when referring to an object with two BPs of opposite topological charge. Another way to interpret this structure is by imagining a stack of two bobbers. In our work, this picture will be the most appropriate due to its capacity to describe the ability of two bobbers to interact. We will thus refer to these structures as bi-bobbers.

Experimental evidence by real-space imaging of bobbers was reported by the means of off-axis electron holography by comparison of skyrmion and bobber contrast.[30] Reciprocal-space imaging to distinguish tube lattices penetrating through the entire specimen and bobber lattices with a termination located well inside the material is reported by quasi-tomographic, resonant, elastic x-ray scattering.[32] Furthermore, a distinction by topological Hall effect measurements is also suggested.[31] Nevertheless, the unambiguous experimental distinction between skyrmion tubes and bobbers or bi-bobbers in systems that cannot be substantially modified to be suitable for resolving the nanoscale magnetization in advanced imaging techniques (e.g., in TEM) is rather challenging. Additionally, in case of isolated objects or missing references for the contrast of bobber and tube, the identification may also be difficult. Most commonly available techniques utilizing static imaging still cannot unambiguously distinguish between the distinct topological fingerprints of more complex objects, as they mostly differ in their projected 2D images, i.e., without the information about the third dimension, so that many topological objects can lead to the same 2D contrast. Especially, spin textures with differing in-plane components will show the same result with 2D projected imaging techniques, but might have different internal modes, as will be useful in another method to distinguish spin textures explained in the next paragraph. It should be noted that with the prospect of new 3D imaging techniques, such as laminography,[36,37] these issues may be overcome in the near future, but this would require large-scale facilities.

On the other hand, a novel and promising all-electrical dynamic method allows for the detection of different magnetic structures based on their unique internal resonance modes.[38] These modes can be excited by periodic external stimuli in the microwave range via a magnetic field,[22,24,39,40] spin torques,[40,41] light,[42] or even by moving skyrmions in nanotracks with periodic constrictions.[43] Internal modes of skyrmionic excitations can be classified as breathing or gyration modes. The former, which will be relevant for this work, is a periodic change of the structure's size resembling the motion of breathing lungs. Depending on the specific magnetic structure, the internal modes can differ in the number of existing resonances, their resonant frequencies, and, most importantly, the dispersion relations as a function of material parameters or, more pertinently, as a function of external fields. Experimental studies of internal modes of skyrmion strings have been successfully conducted using coplanar waveguides and network analyzer ferromagnetic resonance (FMR) setups.[44] Micromagnetic simulation studies on the breathing of skyrmions,[45] antiskyrmions,[46] and synthetic antiferromagnet skyrmions[40] have been reported for frequencies up to 100 GHz. Recently, toron and hopfion breathing modes have been investigated up to 15 GHz.[24]

In this work, a new type of bi-bobber living in a synthetic antiferromagnet (SAF) is introduced. These new bobber systems thus yield additional degrees of freedom in their stacking, which we study with focus on the effects of different chiralities, finding a dependence of the skyrmion stray field on its winding direction. Such a dependence of the strength of a magnetic stray field on the orientation of the magnetic elements producing it is known from certain arrangements of permanent magnets, usually referred to as the so-called Halbach effect.[47,48] It has profound effects on the properties of bi-bobbers. Furthermore, we will compare breathing modes of bi-bobbers and skyrmions in SAFs, excited by periodic out-of-plane magnetic fields with frequencies up to 60 GHz.

II. SIMULATION MODEL

Isolated skyrmionic excitations can be readily studied in disks due to the inherent symmetry of edge states and stray field effects. Thus, we have chosen disk geometry with a diameter of 100 nm and height of 20 nm, which can comfortably accommodate our magnetic textures. Using a cell-size of $1.5625 \times 1.5625 \times 1$ nm^3, a total of $64 \times 64 \times 20$ cells were simulated. For the chiral ferromagnet, an exchange stiffness of $A_{ex} = 7$ pJ m^{-1}, a saturation magnetization of $M_s = 450$ kA m^{-1}, and an interfacial DMI of $D = 2.65$ mJ m^{-2} were chosen, lying between values of other reports for the purpose of comparability.[24,40,45] A perpendicular magnetization anisotropy (PMA) was achieved by setting the out-of-plane uniaxial anisotropy constant to $K_{eff} = 50$ kJ m^{-3}. To stabilize small, geometrically constrained bi-bobbers, we added uniformly magnetized layers at the top and bottom of the simulated stack. For this work, we decided not to fix these layers artificially but, instead, added five layers to the top and bottom with stronger PMA ($K_{eff} = 1$ MJ m^{-3}) and a slightly higher exchange stiffness ($A_{ex} = 20$ pJ m^{-1}). For simulations of the skyrmion tubes, the uniform top and bottom layers were not included to encourage homogeneous tube formation. Also, for better comparability, exchange stiffness and PMA were slightly increased when simulating skyrmion tubes to achieve similar sized tube diameters compared to bobber diameters at the interface.[49] The Gilbert damping coefficient was set as $\alpha = 0.01$ to enable the response in the microwave frequency range.

With this configuration, especially by utilizing an interfacial DMI (iDMI), the simulated model can be thought of as thin films in a multilayered system, sandwiched between two layers of a material with higher PMA and exchange. In this interpretation, each simulation layer can describe a heavy metal/ferromagnet/heavy metal trilayer, which is interconnected to neighboring layers by a combination of direct exchange and stray fields.[50] Alternatively, but experimentally more challenging, our model could also use a sandwiched bulk polar magnet model with C_{nv} symmetry, allowing iDMI and hence the stabilization of Néel skyrmions.[14,15] Nevertheless, fabrication of complex multilayer systems requires sophisticated optimization of the stack. Here, we focus on the fundamental properties of a coupled bobber system as a proof of concept to disentangle different magnetic textures.

For simulations in a synthetic antiferromagnetic environment, the 20 lateral cells were divided into two layers of 10 cells. The two layers directly adjacent to the interface are coupled by the Ruderman–Kittel–Kasuya–Yosida (RKKY) interaction, described by the following contribution to the total micromagnetic energy as readily available[51] in the MuMax3 framework[52] used here:

$$E_{\text{RKKY}} = \frac{\sigma}{d_{\text{NM}}}(1 - \vec{m_1} \cdot \vec{m_2}), \tag{1}$$

with σ being the RKKY interaction coefficient, d_{NM} the thickness of the non-magnetic spacer, which is set to 1 nm in all of our simulations, and $\vec{m_i}$ the normalized magnetization of the top and bottom coupled layers. The RKKY coefficient is set as $\sigma = -2 \times 10^{-4}$ J m^{-2}, lying in the center of a range of values studied for coupled 2D SAF skyrmions.[40] Note that the method used to simulate the SAF disregards the thickness of the spacer layer in the stray field calculation and is geometry dependent due to interactions of the spin textures with edge modes (see the supplementary material). For a direct comparison to experimental results, it can be included at the expense of smaller cells and longer simulation times, and should model the experimentally investigated sample design.[53] To assess the validity of our approach, H–L and L–L bi-bobbers were generated in systems with a gap of 1 nm between the RKKY coupled layers and otherwise the same parameters as stated above. These showed nearly identical bi-bobber energetics as the simulations without gaps.

The magnetization was initialized as Néel-type SAF skyrmion tubes in the chiral layers and as uniform magnetization in the top and bottom high PMA layers, causing the tubes to pinch off and form bobbers. The uniform layers were therefore disregarded for simulations of skyrmion tubes to obtain tubes with a constant diameter throughout the material. Relaxation was performed by integrating an adapted LLG equation, containing only the damping term, using the Runge–Kutta method until a local energy minimum was reached, and a subsequent minimization by the steepest descent method.[52,54]

III. RESULTS

A. Static properties of SAF bi-bobbers

As briefly described before, this work will mainly focus on an antiferromagnetically stacked system of Néel bobbers, and compare their dynamic breathing modes to those of antiferromagnetically coupled Néel skyrmion tubes. Both structures are illustrated in Figs. 1(a) and 1(b), respectively.

The polarity p of skyrmionic excitations is defined as the spin direction of the core. The chirality c is defined by the sense of rotation of the domain wall separating the core from the ferromagnetic background. In SAF environments, the two coupled objects are of opposite polarity, but different combinations of chiralities are possible. As an example, a depiction of $p = -1$ bobbers with right-handed ($c = 1$) and left-handed ($c = -1$) chirality is given in Figs. 1(c) and 1(d), respectively. Experimentally, the sign of c can be chosen in heterostructures by interface engineering.[55,56] An often overlooked effect of skyrmions is their asymmetric stray field, which depends on their chirality. This is illustrated by simulations of the stray field as depicted in Figs. 1(c) and 1(d). The sense of rotation of the latter allows for the stray field to form a closed loop on the top surface, hence lowering the protruding stray field, whereas the former does not. It should be noted that this is reversed at the bottom surface. This effect is well-known on a macroscopic scale, where chiral arrangements of permanent magnets create two opposite surfaces
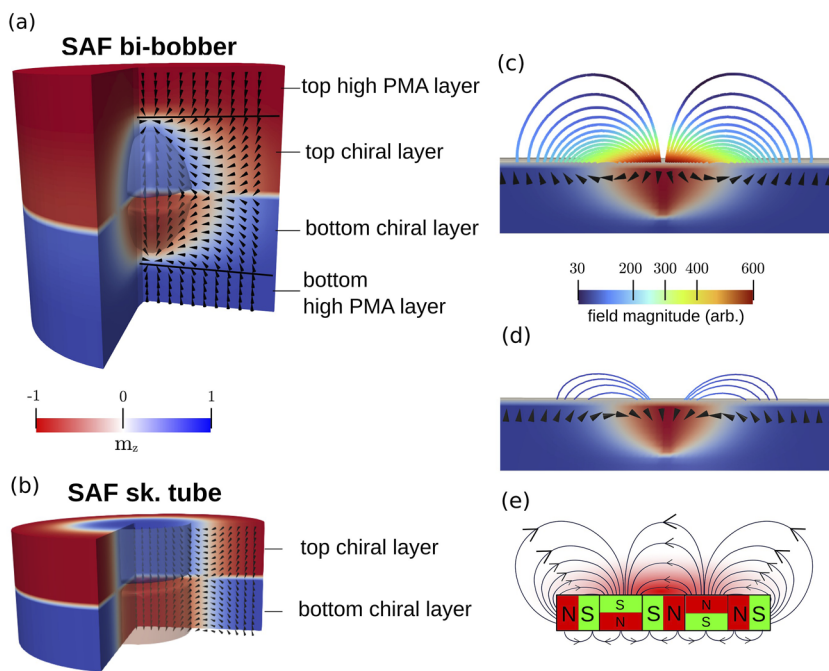

(a) **SAF bi-bobber**
— top high PMA layer
— top chiral layer
— bottom chiral layer
— bottom high PMA layer

(b) **SAF sk. tube**
— top chiral layer
— bottom chiral layer

m_z : -1   0   1

(c)

30   200   300   400   600
field magnitude (arb.)

(d)

(e)

FIG. 1. (a) and (b) Visualization of a SAF bi-bobber and SAF skyrmion tube. (c) and (d) Demonstration of the nanoscale Halbach array for $p = -1$ chiral bobbers with clockwise ($c = 1$) and counterclockwise ($c = -1$) chirality, respectively. (e) Illustration of chiral arrangements of permanent magnets as utilized to create a Halbach array.

with different stray field strengths. An illustration of this is given in Fig. 1(e). On the nanoscale, such effects have been reported and used for the distinction between Bloch and Néel skyrmions by magnetic force microscopy[47,48] but have received little attention when it comes to the interaction of skyrmions living in different magnetic layers. By inspecting Figs. 1(c) and 1(d), four different combinations of stackings with differing stray field interactions become visible. Two symmetric cases, where either both SAF bobbers are of the type shown in Fig. 1(c) and have high invasive stray fields at the interface (H–H), or both are of the type in Fig. 1(d) with low stray fields (L–L). Also, two asymmetric cases with mixed fields are possible, whereas those are just mirror images of one another, i.e., only one needs to be studied (e.g., H–L). This distinction of coupled systems also holds for the simulated skyrmion tubes.

Cross-sections of the simulated layouts are shown in Figs. 1(a) and 1(b). A detailed description of material parameters is given in the modeling section. The top and bottom uniform layers in the bi-bobber sample design have higher PMA and exchange stiffness. They are ferromagnetically coupled to their adjacent chiral layers, while the two chiral blocks are antiferromagnetically coupled through a scaled[51] RKKY-type interaction at their interface [see Eq. (1)]. The ultrathin non-magnetic spacer defining the interface is not simulated. For simulations of the coupled skyrmion tubes, the uniform layers at the very top and bottom were not simulated, as shown in Fig. 1(b).

B. Stability region

To assess the robustness of SAF skyrmions and bi-bobbers, the three different stacking types were first compared to each other in terms of their stability in external fields. This presents the easiest experimental means to judge their properties. Interestingly, the field required to destroy the objects does highly depend on the chirality, or rather the combination of chiralities. Both, SAF bi-bobbers and skyrmion tubes, were the least stable when stacked in the H–H configuration. For the specific set of material parameters chosen for the bi-bobber, even very low external fields of 1 mT are enough to transform them into a single bobber in one layer and a uniform state in the other, i.e., delete one-half of the bi-bobber. For such low fields, the distinction as to which layer transforms to the ferromagnetic state is random. Simulations without stray fields result in stable excitations of the same size in the H–H configuration, confirming that the previously described relaxation to a single bobber is indeed governed by the stray field. Also, in the symmetric cases H–H and L–L, the spins on the domain walls of the skyrmionic objects in the top and bottom layers are not antiferromagnetically aligned. This leads to a higher contribution to the RKKY energy compared to the asymmetric H–L case. However, only in the H–H configuration, strong stray fields of both bobbers (skyrmion tubes) are directly exposed to each other, resembling two repelling magnetic poles, indicating that the symmetric interfacial stray fields destabilize the spin texture. This can be seen even more clearly for the H–H combination of skyrmion tubes, where energy minimization leads to a lateral shift of the coupled skyrmions with respect to one another. In an attempt to obtain non-displaced asymmetric coupled skyrmion tubes, simulations were conducted with higher $\sigma = 1 \cdot 10^{-3}$ J m^{-2} and different skyrmion tube sizes to modify the relative strength of RKKY-coupling and dipole–dipole interaction. However, the stray

field always spatially separated the skyrmion tubes. Therefore, this configuration is omitted in the following analysis.

On the other hand, H–L and L–L combinations were stable for a range of different external fields. A comparison is given in Fig. 2. The bobber diameters in each SAF layer were evaluated at the interface where they reach their highest value. In the H–L configuration, SAF bi-bobbers were stable at fields exceeding 500 mT, whereas in the L–L configuration one of the bobbers was destroyed at 380 mT. Generally, SAF bi-bobber diameters were smaller in the L–L configuration compared to the counterpart values at same external fields in the H–L configuration.
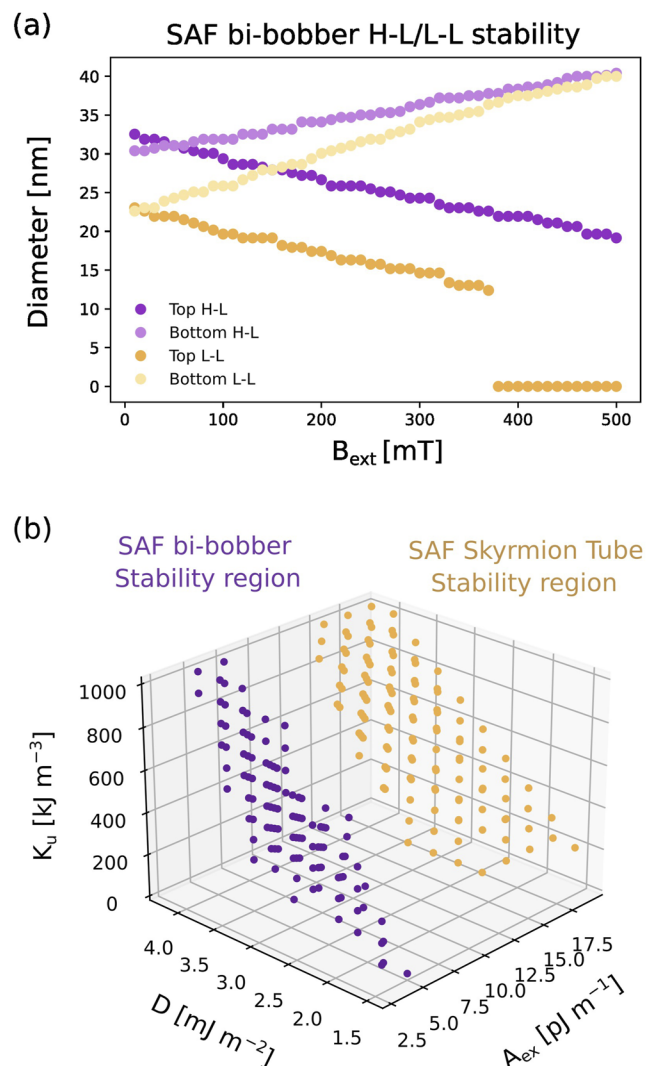

FIG. 2. (a) Diameter of bobbers evaluated in both layers at the SAF interface as a function of external field. The plot gives a comparison between SAF bi-bobbers in an H–L (purple dots) and L–L (orange dots) configuration. (b) Zero-field stability region for SAF bi-bobbers (purple) and SAF skyrmion tubes (orange) for a range of values of D, K_{eff}, and A_{ex}. The dots show the actual simulated data points with stable coupled bobbers or skyrmion tubes. The convex hull is shown as a guide to the eye.

Additionally, the asymmetric stray field has another effect that becomes visible in Fig. 2: In the H–L configuration, the bobber sizes at zero field do not coincide. The above also applies for SAF skyrmion tubes.

Furthermore, to compare the stability between SAF skyrmion tubes and bi-bobbers, zero-field simulations of both were carried out for a reasonable range of material parameters. The parameters of the uniformly magnetized top and bottom layers necessary to stabilize SAF bi-bobbers were not altered. Skyrmionic excitations that exceeded a diameter of 70 nm were considered unstable, since the relaxation of these states in bigger disks leads to constantly increasing skyrmion diameters. Stabilization of these bubbles was mainly attributed to the disk edge and that was not accounted for in the stability region plot.

In Fig. 2(b), the stability comparison is shown for the H–L configurations, which were the most stable for both objects, for ranges of $A_{ex} = (1 - 20)$ pJ m^{-1}, $D = (1.5 - 3.5)$ mJ m^{-2} and K_{eff} = $(1 \cdot 10^1 - 1.1 \cdot 10^3)$ kJ m^{-3}. As can be seen, SAF bi-bobbers approximately have an equal region of stability compared to that of SAF skyrmion tubes within the tested parameter ranges. Due to the proximity of the bi-bobbers to a high exchange and high PMA layer, the stability region of the former shifted toward lower values for A_{ex} and K_{eff} for the chiral layers.

C. Breathing modes

As pointed out earlier, a promising approach to distinguish different types of 3D magnetic textures may be via the excitation of breathing modes. In this section, this breathing mode response to a varying out-of-plane external magnetic field $B_{ac}(t)$ is presented. To quickly and reliably study excitations up to f_{max} = 100 GHz, a sinc pulse-shape is chosen for the AC magnetic field of the following form: $B_{ac}(t) = B_{dc} + B_{ac}^0 \cdot \text{sinc}[2\pi f_{max} \cdot (t - t_0)]$, where B_{dc} is a constant external field offset. Before applying a varying field component, the spin textures were allowed to relax in a field of B_{dc} by the MuMax3 steepest descent minimization method. The field offset guides the initial object size before application of a pulse. Higher offset values will increase the diameter disparity of skyrmionic objects in the antiferromagnetically coupled layers, as already depicted in Fig. 2. Additionally, to eliminate any frequency contribution that might arise due to a relaxation process, a temporal offset of $t_0 = 1$ ns was added to the sinc pulse. An amplitude of $B_{ac}^0 = 0.5$ mT was used for all simulations.

To measure the frequency response, first, the out-of-plane spin component $mz(t)$ was averaged over the full simulated geometry at every simulation time-step. Also, to distinguish between responses of each layer, the top and bottom chiral layers were averaged separately at every simulation time-step. To resolve modes up to 100 GHz, the chosen time-step fulfills the Nyquist–Shannon theorem $\tau_{step} < 1/(2 \cdot 100 \text{ GHz})$. Next, the averaged changes of the out-of-plane spin components $\langle \delta m_z(t) \rangle$ were decomposed into frequency space by Fourier transformation, and the power spectral density (PSD) was computed.

First, the PSD of SAF skyrmion tubes and SAF bi-bobbers in an H–L configuration at fixed external fields are presented for each antiferromagnetically coupled layer in Figs. 3(a)–3(d). As apparent, the resonance modes of SAF bi-bobbers are much richer compared to SAF skyrmion tubes. Since the internal modes of skyrmions depend

on their size,[45] and bobbers contain skyrmions of multiple diameters, this result is in line with our expectations. Figures 3(a) and 3(c) are results at 50 and 20 mT for SAF bi-bobbers and SAF skyrmion tubes, respectively. These are the fields necessary to compensate for the asymmetric stray fields due to the Halbach effect, thus canceling out the size offset of the bobbers or tubes. Hence, with both bobbers and tubes having approximately the same size, their resonances also align. Figures 3(b) and 3(d) show the PSDs at 130 mT. In this configuration, the external field will decrease the magnetic structure size for both bobbers and tubes in the bottom layer, while increasing it in the top layer. As reported for 2D skyrmions, smaller sizes can increase frequencies in a specific band of breathing modes lying around 25 GHz.[45] In our simulations, the peaks start splitting accordingly. It should be noted that the increasing trend of frequencies for smaller skyrmions is not true for all internal modes. As an example of the peak splitting, a zoomed-in plot of the splitting of peaks 2 and 3 is presented for each layer in the inset of Fig. 3(b). Here, it also becomes clearer that frequency responses in one layer also lead to a small peak in the other. For example, the single bobber in the top layer, as plotted in the inset, would not have an additional peak at around 25 GHz. This can be confirmed when viewing the internal mode in Fig. 3(a). Being antiferromagnetically coupled to a smaller bobber resonating at that value triggers this additional response peak. This effect is mutual and appears in both layers. It also appears for coupled skyrmion tubes as can be very clearly seen in Fig. 3(d) at 8 and 19 GHz.

Next, the internal modes are visualized by a cell-by-cell calculation of the PSD. Color-coded cross sections of the results help to get a better understanding of the resonances in real space. Figures 3(e) and 3(f) show the two modes that appeared for the SAF bi-bobber. The figures only show internal modes in the top layer. A mirrored twin of each internal mode can exist in the bottom layer. Every peak in the PSD can be represented by a combination of these modes. Both modes have strong contributions of the BPs. In the mode shown in Fig. 3(e), the layers at the interface with the biggest skyrmion diameter resonate with a comparable strength to the BP. The contribution decreases across the bobber with diminishing skyrmion sizes. In the mode shown in Fig. 3(f), this behavior is reversed. Additionally, a ring outside the bobber participates in the breathing motion, although to a much lower extent. When viewed in a cross-section, this ring is visible as the two lighter spots in Fig. 3(f). As discussed above, none of the internal modes appeared in a single layer. Every resonance triggered a smaller response in its antiferromagnetically coupled neighbor. To illustrate this effect, the full resonance images are shown for two frequencies in Figs. 3(g) and 3(h). None of the resonances was a mixed mode between types shown in Figs. 3(e) and 3(f). In other words, the enforced resonance was always of the same type. All modes were, to a varying degree, hybridized with edge modes,[24,40,45] indicating that the geometry of the sample will need to be taken into account when using this method to distinguish different magnetic textures.

For a direct comparison, Figs. 3(i)–3(k) show the same visualization for the breathing modes of skyrmion tubes at 130 mT. The frequencies at which these were evaluated are highlighted accordingly in Fig. 3(d).

Finally, a full set of PSDs for external fields ranging from 200 mT to 200 mT is depicted as 2D color-coded maps in Fig. 4. With this, dispersion relations are given for all frequencies up to 60 GHz.
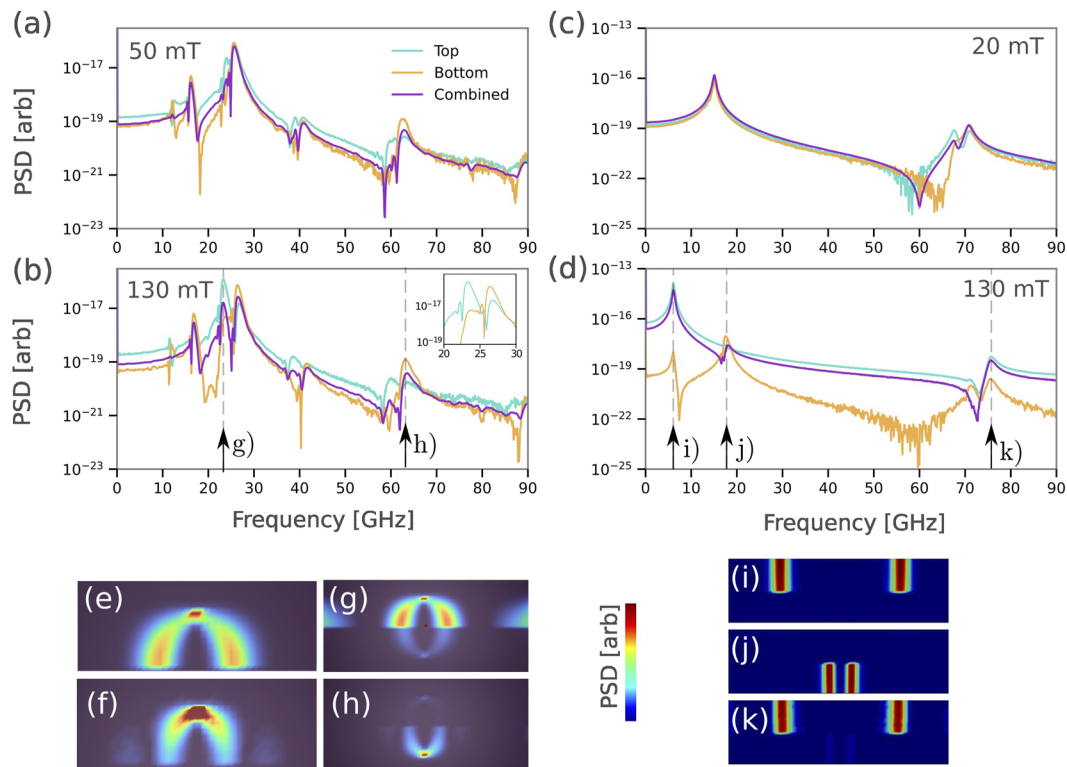
FIG. 3. (a) and (b) Power spectral density of SAF bi-bobbers at 50 mT (stray field compensation point, see main text) and 130 mT, respectively, for the top layer (cyan line), the bottom layer (orange line) and the overall (combined) response (purple line). The inset in (b) is a zoomed-in plot of the frequency range between 20 and 30 GHz, emphasizing the frequency shift between layers at higher external fields and also the mutually enforced frequencies. (c) and (d) Power spectral density of SAF skyrmion tubes at 20 mT (stray field compensation point) and 130 mT, respectively, for different layers with the same color code as used in (a). (e) and (f) Visualization of a cell-by-cell power spectral density evaluation, illustrated in a cross-sectional view and color-coded by the strength of resonance [amplitude of power spectral density (PSD)]. The two panels show the basic modes for the top layer. Note that all other modes are combinations of these two basic modes as shown, e.g., in (g) and (h), for the frequencies highlighted by the respective arrows in panel (b). (i)–(k) Visualization of the cell-by-cell power spectral density for skyrmion tubes at 130 mT at frequencies indicated in panel (d) by vertical dashed lines.

Again, all the effects described earlier can be verified. For the SAF bi-bobber frequency dispersion, as shown in Fig. 4(a), modes 3 and 4 cross at around 50 mT. This is the field at which the asymmetric stray field is compensated, and both bobbers have roughly the same size. The triggered frequency response can be clearly seen in the individual PSDs of each layer, presented in Fig. 4(a) on the left. Modes 1b and 1t fully compensate in the combined plot for fields higher than 60 mT. This means, these specific modes can be driven in a strongly coupled breathing phase by external fields. In this range, both layers breathe with the same amplitude and phase. Note that the symmetry of the cell-by-cell PSD shows the primary components of the oscillations to be breathing modes; however, small contributions produced by gyration might still be present, though undetectable.

When comparing the dispersion of SAF bi-bobber and SAF skyrmion tubes, the strongest bi-bobber resonance modes (3 and 4 in Fig. 4) evolve linearly with the external field, as indicated by the dashed lines for the top and bottom layer in Fig. 4(a) on the left-hand side. Although the skyrmion tube has only two modes in the studied range, the dispersion is more complex. There appears to be

no linear relationship. Furthermore, at −90 and 110 mT, the system is driven into an unstable state. In the usual case of similarly sized tubes, the RKKY energy is minimized by both tubes remaining aligned on top of each other. Here, with the size discrepancy between the two tubes becoming considerably larger. The smaller skyrmion tube can now move within the area of the bigger tube without significant changes in RKKY energy. However, the stray field energy is minimized for the smaller skyrmion tube being as far away from the center of its bigger counterpart as possible. Since nothing is breaking the symmetry in the simulations, very small fields and numerical error can be enough to decide in which direction the small tube will shift. Such lateral shifts have been described before for the H–H configuration. In this state, low frequency gyration modes appear, which are not studied further in this work and may require additional extended investigation. It seems that the frequencies of modes 1 and 2 in this configuration gradually decrease toward zero at −90 and 110 mT, respectively, right before entering the unstable state. Although at higher external fields this strong disparity between the sizes and displacement is still holding, stable breathing modes reappear.
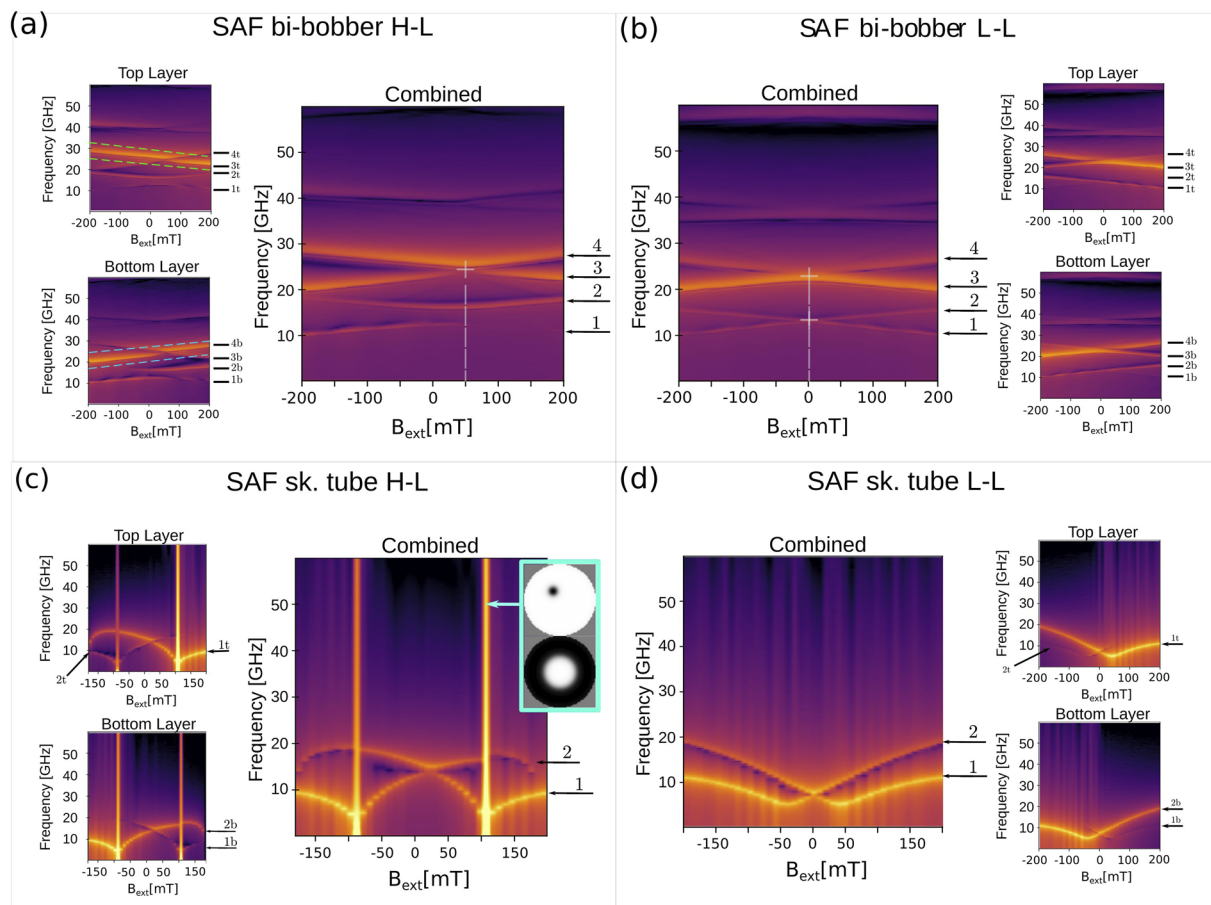
FIG. 4. (a) and (b) Dispersion relations for SAF bi-bobbers in H–L and L–L configurations, respectively. The overall frequency response of all layers combined is shown in the middle, and the internal modes in the top and bottom layers are shown in the respective side panels. The dashed lines in the top and bottom later dispersion relations in panel (a) are guides to the eye, representative of a linear response. (c) Combined dispersion of SAF skyrmion tubes in the H–L configuration, showing a spatial shift of the skyrmion tubes at 110 mT and −90 mT. The gray-scale images show the simulated m_z distributions. (d) Combined dispersion of SAF skyrmion tubes in the H–L configuration.

Additional to previous considerations, Fig. 4 contains simulations for the L–L configuration shown for the SAF bi-bobber and SAF skyrmion tubes in Figs. 4(b) and 4(d), respectively. Due to symmetric stray fields, bobbers or tubes in both SAF layers have the same size at zero-field, and the previously described crossing points shift to 0 mT. Generally, the number of modes is the same for both configurations. Comparing the SAF bi-bobber responses, the L–L configuration modes are shifted toward lower frequencies. Apart from modes 3 and 4, also modes 1 and 2 have a linear response and a crossing point. Other than in the H–L configuration, there is no full compensation of any modes in the studied parameter ranges. SAF skyrmion tube responses do not show the same instability in the L–L case. Frequency minima are reached at lower values of external fields (−50 and 50 mT) and do not decrease toward unstable states. As previously described, this effect is related to the stray field, which is lower in this configuration.

IV. SUMMARY

In this work, we investigated a coupled bi-bobber state in a synthetic antiferromagnetic material that was sandwiched between two uniform ferromagnetic layers. The resulting bobber configurations exhibit strongly chirality-dependent stray fields that cause the coupling to become dependent on the winding orientation of the underlying bobbers, thus affecting the spin texture's stability. This offers a unique platform for the study of collective excitations. We further report that breathing mode excitations provide a valid approach for distinguishing between 3D magnetic textures that otherwise appear very similar.

SUPPLEMENTARY MATERIAL

See the supplementary material for the effects of edge modes and information on the dispersion of saturated states.

AUTHOR DECLARATIONS

Conflict of Interest

The authors have no conflicts to disclose.

Author Contributions

P. Bassirian: Formal analysis (equal); Investigation (equal); Methodology (equal); Writing – original draft (equal); Writing – review & editing (equal). **T. Hesjedal**: Supervision (equal); Writing – original draft (supporting). **S. S. P. Parkin**: Supervision (equal); Writing – original draft (supporting). **K. Litzius**: Project administration (equal); Supervision (equal); Writing – original draft (equal); Writing – review & editing (equal).

DATA AVAILABILITY

The source scripts for bi-bobber breathing can be found publicly available at https://doi.org/10.5281/zenodo.6956156 to be used as reference. The full set of analyzed data that support the findings of this study are available from the corresponding author upon reasonable request.

REFERENCES

[1]Y. Tokura and N. Kanazawa, "Magnetic skyrmion materials," Chem. Rev. **121**, 2857–2897 (2021).

[2]A. Fert, V. Cros, and J. Sampaio, "Skyrmions on the track," Nat. Nanotechnol. **8**, 152–156 (2013).

[3]K. Everschor-Sitte, J. Masell, R. M. Reeve, and M. Kläui, "Perspective: Magnetic skyrmions—Overview of recent progress in an active research field," J. Appl. Phys. **124**, 240901 (2018).

[4]C. Back, V. Cros, H. Ebert, K. Everschor-Sitte, A. Fert, M. Garst, T. Ma, S. Mankovsky, T. L. Monchesky, M. Mostovoy, N. Nagaosa, S. S. P. Parkin, C. Pfleiderer, N. Reyren, A. Rosch, Y. Taguchi, Y. Tokura, K. von Bergmann, and J. Zang, "The 2020 skyrmionics roadmap," J. Phys. D: Appl. Phys. **53**, 363001 (2020).

[5]S. Mühlbauer, B. Binz, F. Jonietz, C. Pfleiderer, A. Rosch, A. Neubauer, R. Georgii, and P. Böni, "Skyrmion lattice in a chiral magnet," Science **323**, 915–919 (2009).

[6]X. Z. Yu, Y. Onose, N. Kanazawa, J. H. Park, J. H. Han, Y. Matsui, N. Nagaosa, and Y. Tokura, "Real-space observation of a two-dimensional skyrmion crystal," Nature **465**, 901–904 (2010).

[7]W. Münzer, A. Neubauer, T. Adams, S. Mühlbauer, C. Franz, F. Jonietz, R. Georgii, P. Böni, B. Pedersen, M. Schmidt, A. Rosch, and C. Pfleiderer, "Skyrmion lattice in the doped semiconductor $Fe_{1-x}Co_xSi$," Phys. Rev. B **81**, 041203 (2010).

[8]K. Litzius, I. Lemesh, B. Krüger, P. Bassirian, L. Caretta, K. Richter, F. Büttner, K. Sato, O. A. Tretiakov, J. Förster, R. M. Reeve, M. Weigand, I. Bykova, H. Stoll, G. Schütz, G. S. D. Beach, and M. Kläui, "Skyrmion hall effect revealed by direct time-resolved x-ray microscopy," Nat. Phys. **13**, 170–175 (2016).

[9]I. Lemesh, K. Litzius, M. Böttcher, P. Bassirian, N. Kerber, D. Heinze, J. Zázvorka, F. Büttner, L. Caretta, M. Mann, M. Weigand, S. Finizio, J. Raabe, M. Y. Im, H. Stoll, G. Schütz, B. Dupé, M. Kläui, and G. S. D. Beach, "Current-induced skyrmion generation through morphological thermal transitions in chiral ferromagnetic heterostructures," Adv. Mater. **30**, 1805461 (2018).

[10]L. Wang, Q. Feng, Y. Kim, R. Kim, K. H. Lee, S. D. Pollard, Y. J. Shin, H. Zhou, W. Peng, and D. Lee, "Ferroelectrically tunable magnetic skyrmions in ultrathin oxide heterostructures," Nat. Mater. **17**, 1087–1094 (2018).

[11]A. Yagil, A. Almoalem, A. Soumyanarayanan, A. K. C. Tan, M. Raju, C. Panagopoulos, and O. M. Auslaender, "Stray field signatures of Néel textured skyrmions in Ir/Fe/Co/Pt multilayer films," Appl. Phys. Lett. **112**, 192403 (2018).

[12]C. Moreau-Luchaire, C. Moutafis, N. Reyren, J. Sampaio, C. A. F. Vaz, N. Van Horne, K. Bouzehouane, K. Garcia, C. Deranlot, P. Warnicke, P. Wohlhüter, J.-M. George, M. Weigand, J. Raabe, V. Cros, and A. Fert, "Additive interfacial chiral interaction in multilayers for stabilization of small individual skyrmions at room temperature," Nat. Nanotechnol. **11**, 444–448 (2016).

[13]S. Zhang, J. Zhang, Y. Wen, Y. Peng, Z. Qiu, T. Matsumoto, and X. Zhang, "Deformation of Néel-type skyrmions revealed by Lorentz transmission electron microscopy," Appl. Phys. Lett. **116**, 142402 (2020).

[14]T. Kurumaji, T. Nakajima, V. Ukleev, A. Feoktystov, T.-h. Arima, K. Kakurai, and Y. Tokura, "Néel-type skyrmion lattice in the tetragonal polar magnet $VOSe_2O_5$," Phys. Rev. Lett. **119**, 237201 (2017).

[15]A. K. Srivastava, P. Devi, A. K. Sharma, T. Ma, H. Deniz, H. L. Meyerheim, C. Felser, and S. S. P. Parkin, "Observation of robust Néel skyrmions in metallic PtMnGa," Adv. Mater. **32**, 1904327 (2020).

[16]S. Zhang, G. van der Laan, J. Müller, L. Heinen, M. Garst, A. Bauer, H. Berger, C. Pfleiderer, and T. Hesjedal, "Reciprocal space tomography of 3D skyrmion lattice order in a chiral magnet," Proc. Natl. Acad. Sci. U.S.A. **115**, 6386–6391 (2018).

[17]B. Göbel, I. Mertig, and O. A. Tretiakov, "Beyond skyrmions: Review and perspectives of alternative magnetic quasiparticles," Phys. Rep. **895**, 1–28 (2021).

[18]T. Yokouchi, S. Hoshino, N. Kanazawa, A. Kikkawa, D. Morikawa, K. Shibata, T. H. Arima, Y. Taguchi, F. Kagawa, N. Nagaosa, and Y. Tokura, "Current-induced dynamics of skyrmion strings," Sci. Adv. **4**, eaat1115 (2018).

[19]M. T. Birch, D. Cortés-Ortuño, L. A. Turnbull, M. N. Wilson, F. Groß, N. Träger, A. Laurenson, N. Bukin, S. H. Moody, M. Weigand, G. Schütz, H. Popescu, R. Fan, P. Steadman, J. A. T. Verezhak, G. Balakrishnan, J. C. Loudon, A. C. Twitchett-Harrison, O. Hovorka, H. Fangohr, F. Y. Ogrin, J. Gräfe, and P. D. Hatton, "Real-space imaging of confined magnetic skyrmion tubes," Nat. Commun. **11**, 1726 (2020).

[20]S. Seki, M. Suzuki, M. Ishibashi, R. Takagi, N. D. Khanh, Y. Shiota, K. Shibata, W. Koshibae, Y. Tokura, and T. Ono, "Direct visualization of the three-dimensional shape of skyrmion strings in a noncentrosymmetric magnet," Nat. Mater. **21**, 181–187 (2021).

[21]K. Ran, Y. Liu, H. Jin, Y. Shangguan, Y. Guang, J. Wen, G. Yu, G. van der Laan, T. Hesjedal, and S. Zhang, "Axially bound magnetic skyrmions: Glueing topological strings across an interface," Nano Lett. **22**, 3737 (2022).

[22]Y. Liu, R. K. Lake, and J. Zang, "Binding a hopfion in a chiral magnet nanodisk," Phys. Rev. B **98**, 174437 (2018).

[23]N. Kent, N. Reynolds, D. Raftrey, I. T. G. Campbell, S. Virasawmy, S. Dhuey, R. V. Chopdekar, A. Hierro-Rodriguez, A. Sorrentino, E. Pereiro, S. Ferrer, F. Hellman, P. Sutcliffe, and P. Fischer, "Creation and observation of hopfions in magnetic multilayer systems," Nat. Commun. **12**, 1562 (2021).

[24]D. Raftrey and P. Fischer, "Field-driven dynamics of magnetic hopfions," Phys. Rev. Lett. **127**, 257201 (2021).

[25]F. Zheng, F. N. Rybakov, N. S. Kiselev, D. Song, A. Kovács, H. Du, S. Blügel, and R. E. Dunin-Borkowski, "Magnetic skyrmion braids," Nat. Commun. **12**, 5316 (2021).

[26]P. J. Ackerman and I. I. Smalyukh, "Static three-dimensional topological solitons in fluid chiral ferromagnets and colloids," Nat. Mater. **16**, 426–432 (2016).

[27]S. Grytsiuk, J.-P. Hanke, M. Hoffmann, J. Bouaziz, O. Gomonay, G. Bihlmayer, S. Lounis, Y. Mokrousov, and S. Blügel, "Topological chiral magnetic interactions driven by emergent orbital magnetism," Nat. Commun. **11**, 511 (2020).

[28]P. Sutcliffe, "Skyrmion knots in frustrated magnets," Phys. Rev. Lett. **118**, 247203 (2017).

[29]F. N. Rybakov, A. B. Borisov, S. Blügel, and N. S. Kiselev, "New type of stable particle like states in chiral magnets," Phys. Rev. Lett. **115**, 117201 (2015).

[30]F. Zheng, F. N. Rybakov, A. B. Borisov, D. Song, S. Wang, Z.-A. Li, H. Du, N. S. Kiselev, J. Caron, and A. Kovács, "Experimental observation of chiral magnetic bobbers in B20-type FeGe," Nat. Nanotechnol. **13**, 451–455 (2018).

[31]A. S. Ahmed, J. Rowland, B. D. Esser, S. R. Dunsiger, D. W. McComb, M. Randeria, and R. K. Kawakami, "Chiral bobbers and skyrmions in epitaxial FeGe/Si(111) films," Phys. Rev. Mater. **2**, 041401 (2018).

[32]K. Ran, Y. Liu, Y. Guang, D. M. Burn, G. van der Laan, T. Hesjedal, H. Du, G. Yu, and S. Zhang, "Creation of a chiral bobber lattice in helimagnet-multilayer heterostructures," Phys. Rev. Lett. **126**, 017204 (2021).

[33]A. O. Leonov and K. Inoue, "Homogeneous and heterogeneous nucleation of skyrmions in thin layers of cubic helimagnets," Phys. Rev. B **98**, 054404 (2018).

[34]S. Ostlund, "Interactions between topological point singularities," Phys. Rev. B **24**, 485–488 (1981).

[35]G. P. Müller, F. N. Rybakov, H. Jónsson, S. Blügel, and N. S. Kiselev, "Coupled quasimonopoles in chiral magnets," Phys. Rev. B **101**, 184405 (2020).

[36]C. Donnelly, S. Finizio, S. Gliga, M. Holler, A. Hrabec, M. Odstrčil, S. Mayr, V. Scagnoli, L. J. Heyderman, and M. Guizar-Sicairos, "Time-resolved imaging of three-dimensional nanoscale magnetization dynamics," Nat. Nanotechnol. **15**, 356–360 (2020).

[37]S. Finizio, C. Donnelly, S. Mayr, A. Hrabec, and J. Raabe, "Three-dimensional vortex gyration dynamics unraveled by time-resolved soft x-ray laminography with freely selectable excitation frequencies," Nano Lett. **22**, 1971–1977 (2022).

[38]M. Lonsky and A. Hoffmann, "Dynamic excitations of chiral magnetic textures," APL Mater. **8**, 100903 (2020).

[39]J. Kim, J. Yang, Y.-J. Cho, B. Kim, and S.-K. Kim, "Coupled breathing modes in one-dimensional skyrmion lattices," J. Appl. Phys. **123**, 053903 (2018).

[40]M. Lonsky and A. Hoffmann, "Coupled skyrmion breathing modes in synthetic ferri- and antiferromagnets," Phys. Rev. B **102**, 104403 (2020).

[41]S. Woo, K. M. Song, K.-S. Han, M.-S. Jung, M.-Y. Im, K.-S. Lee, K. S. Song, P. Fischer, J.-I. Hong, and J. W. Choi, "Spin-orbit torque-driven skyrmion dynamics revealed by time-resolved x-ray microscopy," Nat. Commun. **8**, 15573 (2017).

[42]N. Ogawa, S. Seki, and Y. Tokura, "Ultrafast optical excitation of magnetic skyrmions," Sci. Rep. **5**, 9552 (2015).

[43]J. Leliaert, P. Gypens, M. V. Milošević, B. Van Waeyenberge, and J. Mulkers, "Coupling of the skyrmion velocity to its breathing mode in periodically notched nanotracks," J. Phys. D: Appl. Phys. **52**, 024003 (2018).

[44]S. Seki, M. Garst, J. Waizner, R. Takagi, N. D. Khanh, Y. Okamura, K. Kondou, F. Kagawa, Y. Otani, and Y. Tokura, "Propagation dynamics of spin excitations along skyrmion strings," Nat. Commun. **11**, 256 (2020).

[45]J.-V. Kim, F. Garcia-Sanchez, J. a. Sampaio, C. Moreau-Luchaire, V. Cros, and A. Fert, "Breathing modes of confined skyrmions in ultrathin magnetic dots," Phys. Rev. B **90**, 064410 (2014).

[46]X. J. Liu, L. Guo, H. Wang, and Z. K. Tang, "The internal dynamic modes of an antiskyrmion in ultrathin ferromagnetic nanodisks," AIP Adv. **10**, 075222 (2020).

[47]M. A. Marioni, M. Penedo, M. Baćani, J. Schwenk, and H. J. Hug, "Halbach effect at the nanoscale from chiral spin textures," Nano Lett. **18**, 2263–2267 (2018).

[48]K.-Y. Meng, A. S. Ahmed, M. Baćani, A.-O. Mandru, X. Zhao, N. Bagués, B. D. Esser, J. Flores, D. W. McComb, H. J. Hug, and F. Yang, "Observation of nanoscale skyrmions in SrIrO$_3$/SrRuO$_3$ bilayers," Nano Lett. **19**, 3169–3175 (2019).

[49]The altered parameters for the tube simulation to obtain identical bobber and tube diameters were K_{eff} = 600 kJ m^{-3} and A_{ex} = 12 pJ m^{-1} (opposite DMI) or A_{ex} = 15 pJ m^{-1} (same DMI).

[50]S. Woo, K. Litzius, B. Krüger, M.-Y. Im, L. Caretta, K. Richter, M. Mann, A. Krone, R. M. Reeve, M. Weigand, P. Agrawal, I. Lemesh, M.-A. Mawass, P. Fischer, M. Kläui, and G. S. D. Beach, "Observation of room-temperature magnetic skyrmions and their current-driven dynamics in ultrathin metallic ferromagnets," Nat. Mater. **15**, 501–506 (2016).

[51]J. De Clercq, J. Leliaert, and B. Van Waeyenberge, "Modelling compensated antiferromagnetic interfaces with MuMax3," J. Phys. D: Appl. Phys. **50**, 425002 (2017).

[52]A. Vansteenkiste, J. Leliaert, M. Dvornik, M. Helsen, F. Garcia-Sanchez, and B. Van Waeyenberge, "The design and verification of MuMax3," AIP Adv. **4**, 107133 (2014).

[53]W. Legrand, D. Maccariello, F. Ajejas, S. Collin, A. Vecchiola, K. Bouzehouane, N. Reyren, V. Cros, and A. Fert, "Room-temperature stabilization of antiferromagnetic skyrmions in synthetic antiferromagnets," Nat. Mater. **19**, 34–42 (2019).

[54]L. Exl, S. Bance, F. Reichel, T. Schrefl, H. Peter Stimming, and N. J. Mauser, "LaBonte's method revisited: An effective steepest descent method for micromagnetic energy minimization," J. Appl. Phys. **115**, 17D118 (2014).

[55]G. Chen, T. Ma, A. T. N'Diaye, H. Kwon, C. Won, Y. Wu, and A. K. Schmid, "Tailoring the chirality of magnetic domain walls by interface engineering," Nat. Commun. **4**, 2671 (2013).

[56]A. Hrabec, J. Sampaio, M. Belmeguenai, I. Gross, R. Weil, S. M. Chérif, A. Stashkevich, V. Jacques, A. Thiaville, and S. Rohart, "Current-induced skyrmion generation and dynamics in symmetric bilayers," Nat. Commun. **8**, 15765 (2017).